A METHOD FOR DRAG DECOMPOSITION FROM CFD CALCULATIONS

Luigi Paparone, Renato Tognaccini
CIRA Centro Italiano Ricerche Aerospaziali, Capua (CE), Italy,
l.paparone@cira.it.
Dipartimento di Progettazione Aeronautica,
Università di Napoli Federico II, Napoli, Italy,
renato.tognaccini@unina.it.

Keywords: *CFD, aerodynamic drag*

Abstract

A method for the computation and breakdown of the aerodynamic drag into viscous and wave components is here proposed. Relying on a given numerical solution of the Reynolds Averaged Navier-Stokes equations, the method allows for the determination of the drag related to entropy variations in the flow. The identification of a spurious contribution due to the numerical dissipation of the flow solver algorithm allows for drag computations weakly dependent on mesh size. By this method accurate drag calculations are possible even on moderately sized grids. Results are presented for transonic flows around an airfoil and a wing-body configuration.

1 Introduction

The problem of drag extraction from CFD calculations is still open today, and much research has been devoted to this subject. The interested reader can find an initial review with fundamentals of physics in [1, 2], while recently an extended and detailed overview of the state of the art on drag prediction methods has been given in [3].

The numerical computation of drag by surface integration of stresses (near field method) usually gives insufficiently accurate results even if the flow solution is locally accurate (in terms of pressure and velocity profiles for instance). In particular for numerical solutions of the Reynolds Averaged Navier-Stokes (RANS) equations, which are discussed in this work, the problem is mainly related to the presence of the numerical artificial dissipation which produces an artificial or "spurious" drag. This contribution becomes negligible only for not feasible calculations with infinitely dense grids.

A second problem concerns the fact that the near field drag computation only allows for a distinction between "pressure" and "friction" drag. Additional useful information would be the breakdown into other physical components, such as viscous drag (associated with boundary layers), wave drag (associated with possible shock waves in transonic and supersonic flows) and lift induced or vortex drag (associated with the free vortex system shedding from 3D lifting bodies). This task is relatively simple when drag has to be extracted by classical viscous-inviscid interaction methods. On the contrary, in the case of analysis performed by RANS methods such as in wind tunnel experiments, the physical drag source is not isolated and the breakdown into individual components becomes difficult. In practice, for a real flow there is not a clear definition of the different drag contributions.

In the present work a solution to these problems is proposed when the drag associated with entropy production in a RANS solution is considered. This "entropy drag" is made up of viscous and wave components and it represents the total drag for 2D adiabatic flows.

The proposed method is based on a far field approach in which the drag is determined from the momentum integral balance by considering fluxes evaluated on a surface far from the body.

Oswatitsch [4] derived a far field formula of the entropy drag considering first order effects, in which the drag is expressed as the flux of a function only dependent on entropy variations. Lock [5] used the Oswatitsch's formula for computing the wave drag in inviscid flows in terms of entropy jumps across the shocks. In [6] and [7] the Oswatitsch's formula is used for computing the entropy drag in RANS solutions by limiting the far field flux computation to a box enclosing the aircraft. However this method does not eliminate the error due to the spurious drag, which is mostly concentrated near the configuration (where larger flow gradients and grid metric variations are present) and does not allow for the breakdown into constituent drag components. Indeed when fluxes are computed on surfaces far from the configuration, it is difficult to distinguish between wave and viscous contributions for streamlines crossing both the inviscid shock and the boundary layer. This is a major problem for the breakdown of drag by far field methods as noted in [2].

In [8] a viscous and a wave drag contribution for a transonic airfoil flow has been computed by separately applying the Oswatitsch's formula in the boundary layer wake and just aft the shock wave. Nevertheless this method seems difficult to extend to the analysis of complex 3D flows and again, does not account for spurious drag contributions.

An interesting idea was exploited in [9] for inviscid Euler flows. Gauss's theorem allows for the replacement of the surface integral in the Oswatitsch's formula with a volume integral; therefore the integrand can be set to zero "a priori" in regions where it is known that physical entropy variations should be zero, thus removing spurious contributions to drag.

In the following sections a general far field expression of drag by Taylor's series expansion with respect to entropy, pressure and total enthalpy variations is derived. In this way the entropy contribution can be separated from the drag due to lift. The first order term is coincident with the Oswatitsch's formula; it is shown, by numerical experiments, that for viscous flows this term is not sufficient for accurate drag prediction and the additional second order term is at least required.

The entropy drag is then expressed in terms of a volume integral that can be easily computed. In such a way it is possible to split drag into wave and viscous contributions once the shock wave and the boundary layer/wake regions are properly identified. In addition, following [9], the spurious term associated with the volume integration in the remaining part of the flow can be eliminated, allowing for accurate drag predictions with medium sized grids.

This method has been used to derive the lift versus drag curves of an airfoil. The results obtained in the case of transonic flow are presented and compared with experiments. In addition the feasibility of the method to compute and split drag for complex flows is shown by presenting the breakdown of drag at different lifts obtained for a wing-body configuration in transonic flow conditions.

2 The far field drag definition

It is here considered a steady fluid flow with free stream velocity V_∞ around an unpowered aircraft configuration, implying that the only external force acting on the body is due to the fluid. The integral formulation of the momentum balance for a volume Ω surrounding the

body leads to

$$\int_S [(\rho\vec{V}\vec{V})\cdot\vec{n} + p\vec{n} - (\vec{\vec{\tau}}\cdot\vec{n})]dS = 0. \quad (1)$$

ρ, $\vec{V}$, p and $\vec{\vec{\tau}}$ specify respectively the density, velocity vector, static pressure and the viscous stress tensor. S is the surface bounding the volume Ω and $\vec{n}$ is the unit normal vector pointing outside the volume Ω. If the surface S is decomposed as $S = S_{body} \bigcup S_{far}$ with S_{body} specifying the body surface and S_{far} the external surface bounding the volume Ω, it is possible to obtain the total force acting on the body:

$$\begin{aligned}\vec{F}_{body} &= \int_{S_{body}} [p\vec{n} - (\vec{\vec{\tau}}\cdot\vec{n})]dS \\ &= -\int_{S_{far}} [(\rho\vec{V}\vec{V})\cdot\vec{n} + \\ &\quad p\vec{n} - (\vec{\vec{\tau}}\cdot\vec{n})]dS. \end{aligned} \quad (2)$$

This equation shows that the body force can be evaluated through two different approaches:

1. by performing an integral of the acting stress on the body surface (first integral of the (2)): *near field method*;

2. by calculating the second integral of the (2), i.e. by evaluating the net momentum flux across the surface S_{far}: *far field method*.

With reference to a Cartesian system $(Oxyz)$ with the x-axis aligned with the free stream velocity vector, the far field drag expression can be obtained by projecting the second integral of equation (2) in the x-direction

$$\begin{aligned}D_{far} &= -\int_{S_{far}} [pn_x + \rho u(\vec{V}\cdot\vec{n}) - \\ &\quad \tau_{xx}n_x - \tau_{xy}n_y - \tau_{xz}n_z]dS. \end{aligned} \quad (3)$$

If the surface S_{far} is chosen infinitely far from the body ($S_{far,\infty}$) it is possible to neglect the viscous stress terms in the expression (3). Furthermore it can be proved [10] that, in the case of 2D flows, the far field drag expression can be further simplified since, in this case, the contribution of the pressure to the integral of equation (3) vanishes, thus obtaining

$$D_{far} = -\int_{S_{far,\infty}} \rho V(\vec{V}\cdot\vec{n})dS. \quad (4)$$

By the definitions of total enthalpy and entropy of a perfect gas it is possible to express the module of the velocity in terms of variations of total enthalpy (ΔH), entropy (Δs) and static pressure (Δp) with respect to the free stream values. If the total enthalpy variation is neglected (it is very small for a flow with Prandtl number nearly equal to one)

$$D_{far} = -V_\infty \int_{S_{far,\infty}} \rho(\vec{V}\cdot\vec{n})\sqrt{1-g}dS, \quad (5)$$

where

$$\begin{aligned}g &= \frac{2}{(\gamma-1)M_\infty^2}\cdot \\ &\quad \left\{\left[(\Delta p + 1)\, e^{\frac{\Delta s}{R}}\right]^{\frac{(\gamma-1)}{\gamma}} - 1\right\}, \end{aligned} \quad (6)$$

with R and γ respectively the gas constant and the specific heat ratio of air. In 2D flows the drag formula (5) provides an "exact" expression in terms of the entropy variation in the flow.

3 Entropy drag and its breakdown

The 3D far field drag expression (4) can be manipulated [10] by considering the already cited expression of the velocity module and performing a Taylor series expansion in terms of Δs, Δp and ΔH. Considering first and second order terms associated with entropy variation, the expression of the entropy drag coefficient in a general 3D flow becomes (the drag coefficient C_D is here used)

$$\begin{aligned}C_D &= \frac{2}{\gamma M_\infty^2}\int_{S_{far}} \left\{\frac{\Delta s}{R} + \right. \\ &\quad \left.\left[\frac{1+(\gamma-1)M_\infty^2}{2\gamma M_\infty^2}\right]\left(\frac{\Delta s}{R}\right)^2\right\}\cdot \\ &\quad \hat{\rho}(\vec{\hat{V}}\cdot\vec{n})d\hat{S}. \end{aligned} \quad (7)$$

The symbol $\hat{}$ specifies non dimensional quantities, and v_i is the x-component of the unit versor of V_∞. The integral in the expression (7) is connected with the entropy rise $\frac{\Delta s}{R}$ on S_{far}; it is here defined as the entropy drag around a 3D unpowered aircraft configuration. The first order contribution of the entropy drag is equal to the well known drag expression derived by Oswatitsch [4] widely used especially in the computation of the wave drag in inviscid flows.

As stated in the introduction the drag breakdown procedure is ambiguous for a real flow. Another problem is related to the presence in the numerical solutions of artificial dissipation terms (explicit or implicit) which add a "spurious" or "numerical" contribution to the computed drag despite its computation by a near or far field method.

By the Gauss theorem the entropy drag in equation (7) can be written in the form (on the body surface $\vec{V} \cdot \vec{n} = 0$)

$$C_D = \frac{2}{\gamma M_\infty^2} \int_\Omega \vec{\nabla} \cdot [f(\frac{\Delta s}{R}) \rho \vec{V}] \, d\Omega, \qquad (8)$$

where $f(\frac{\Delta s}{R})$ is given by the term in braces in the integral of (7).

The domain Ω can be decomposed as $\Omega = \Omega_{bl} \bigcup \Omega_w \bigcup \Omega_s$. Ω_{bl} is the volume containing the boundary layer and the viscous wake, Ω_w contains the shock wave, and Ω_s specifies the remaining part of the flow field. Hence by the relation (8) the entropy drag can be expressed as the sum of three contributions:

$$\begin{aligned} C_D \;=\; & \frac{2}{\gamma M_\infty^2} \left\{ \int_{\Omega_{bl}} \vec{\nabla} \cdot [f(\frac{\Delta s}{R}) \rho \vec{V}] \, d\Omega + \right. \\ & \int_{\Omega_w} \vec{\nabla} \cdot [f(\frac{\Delta s}{R}) \rho \vec{V}] \, d\Omega + \\ & \left. \int_{\Omega_s} \vec{\nabla} \cdot [f(\frac{\Delta s}{R}) \rho \vec{V}] \, d\Omega \right\}. \qquad (9) \end{aligned}$$

Each integral in the expression (9) is connected with the entropy production in the corresponding volume Ω_i. Thus by equation (9) it is possible to write $C_D = C_{D_{bl}} + C_{D_w} + C_{D_{sp}}$, respectively the viscous, wave and spurious drag coefficients. Since $C_{D_{bl}}$ and C_{D_w} are also affected by spurious contributions $C_{D_{sp}}$ cannot represent the total unphysical drag, although hopefully its detection and elimination can reduce the dependency of the computed drag on the grid density.

3.1 Algortithms for regions selection

It is clear that the proposed entropy drag breakdown relies on a proper definition of the boundary layer and shock region. For such purpose a zone selection algorithm has been developed, based on the physical features of the flow field. The problem to be considered is to establish whether a grid cell, for which all thermofluidynamic information are known, belongs to the boundary layer, to the shock wave or to the remaining part of the flow domain. The selection algorithm becomes critical in shock wave - boundary layer interaction zones because there it is not clear the distinction (both theoretical and practical) between boundary layer and shock.

The automatic selection of the shock wave region relies on a sensor based on the following non dimensional function:

$$F_{shock} = \frac{\mathbf{V} \cdot \nabla p}{a |\nabla p|}, \qquad (10)$$

where a is the local sound speed. This sensor is negative in expansion zones (where obviously shock waves are not present) and positive in compression regions. Thus, cells with negative values of F_{shock} can be automatically excluded from the shock wave region.

A further selection can be made because this sensor gives a guess of the local Mach number component in the direction of the pressure gradient. $F_{shock} > 1$ in the compression zone, implies that the corresponding cell is in the neighborhood (upwind) of a shock wave. Furthermore by using the Rankine-Hugoniot relations it is also possible to get an estimation of the Mach number downstream of the shock. This value can be used as a cut-off (F_{cw}) for the shock function and allows to

select cells both upstream and downstream of the shock wave if the test $F_{shock} > F_{cw}$ is satisfied.

The identification of a proper automatic sensor for the detection of the boundary layer and wake required larger efforts. A first difficulty is given by the requirement of a topology independent selection criteria to allow for an algorithm independent on the configuration and also applicable to unstructured data. Therefore a sensor based on the boundary layer thickness (which on the other hand is ambiguous and strongly dependent on a cutoff value) cannot be used. Furthermore the sensors cannot be based on variables related to the entropy production, for instance the dissipation of kinetic energy, because they tend to also detect the spurious region. In the present work it has been introduced a sensor properly working for fully turbulent flows. In this case the eddy viscosity is a reliable measure of the relevance of the viscous effects. The adopted sensor is:

$$F_v = \frac{\mu_l + \mu_t}{\mu_l}, \qquad (11)$$

where μ_l and μ_t are respectively the dynamic and eddy viscosity. The value of F_v is very high in the boundary layer and wake while is ≈ 1 in the remaining part of the domain. The viscous region is selected by checking if $F_v > 1.1 \cdot F_{v\infty}$, where $F_{v\infty}$ the free stream value of the boundary layer sensor.

4 Results

The flow simulations, which are the basis for the drag analysis, have been obtained solving on block structured grids the steady RANS equations, by a standard technique based on the well known central space discretization, with self adaptive explicit second and fourth order artificial dissipation [12]. Two turbulence models have been used, the Baldwin-Lomax [13] for the 2D test and the Spalart-Allmaras [14] for the wing-body test.

4.1 2D airfoil

The polar curve (C_L vs C_D) of the NACA 0012 airfoil has been computed at free stream conditions $M_\infty = 0.7$, $Re_\infty = 9 \cdot 10^6$ (an experimental data set can be found in [15]). The mesh is a single-block C-type grid with four grid levels, made up respectively of 80 x 32 (coarse), 160 x 64 (medium), 320 x 128 (fine), and 640 x 256 (superfine) cells.

The surface pressure distributions on the medium, fine and superfine grid are compared with the experiments at $C_L = 0.5$ in figure 1. The agreement is satisfactory both in terms of pressure peak and shock wave location.

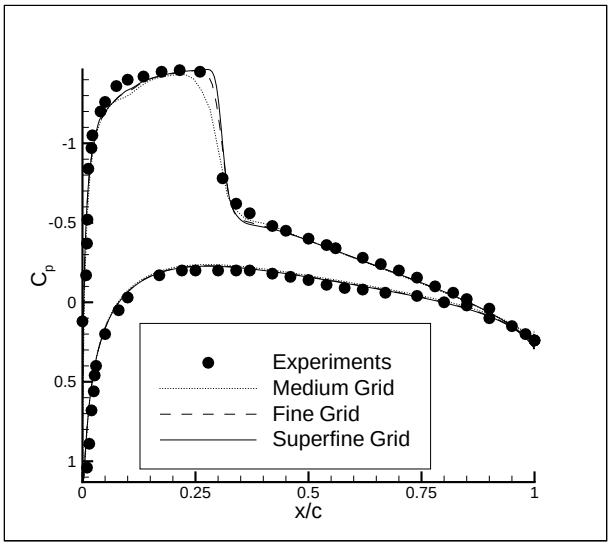

Fig. 1 NACA 0012, viscous test, surface pressure distributions, $M_\infty = 0.7$, $Re_\infty = 9 \cdot 10^6$, $C_L = 0.5$.

The viscous and wave drag computed by using the formula (7), respectively with the 1^{st} and the 2^{nd} order entropy terms and by using the exact formula (5) have been compared. The 2^{nd} order approximation agrees with the relation (5) for both viscous and wave drag. On the contrary the 1^{st} order approximation underestimate viscous drag of 3%. This is caused by the entropy variations in the boundary layer which are larger than the variations across shock waves. Therefore, in the following, the far field C_D is always computed by

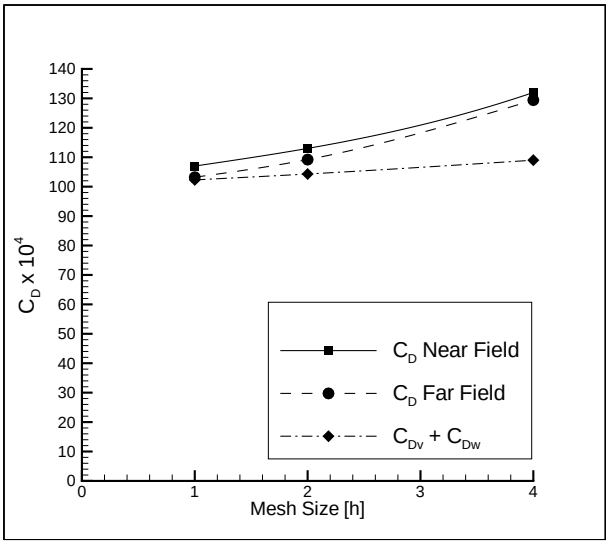

Fig. 2 NACA 0012, viscous test, far field C_D versus mesh size, $M_\infty = 0.7$, $Re_\infty = 9 \cdot 10^6$, $C_L = 0.424$.

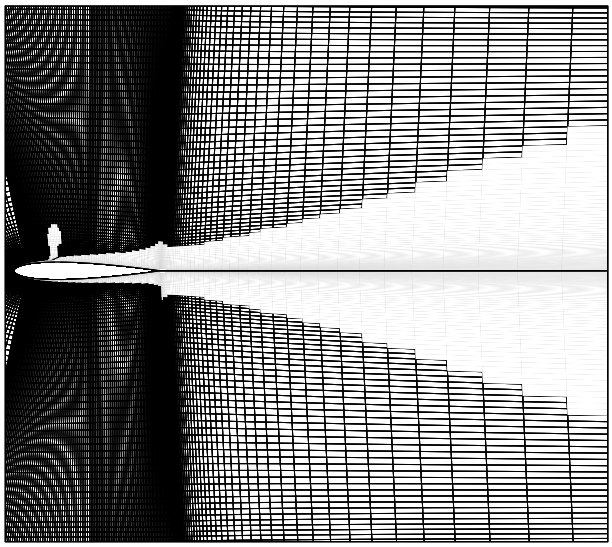

Fig. 3 NACA 0012, viscous test, viscous region selected in the fine grid test, $M_\infty = 0.7$, $Re_\infty = 9 \cdot 10^6$, $C_L = 0.424$.

retaining the 2^{nd} order approximation.

The application of the breakdown algorithm allows for the identification of a spurious contribution that can be removed from the drag computation, and the drag variation with the mesh size is considerably reduced, see figure 2 for the C_L=0.424 case; In this test the spurious drag ($C_{D_{sp}}$) ranges from 20 counts (h=4 grid) to 1 count (h=1 grid) and $C_{D_v} + C_{D_w}$ only differs 7 counts among tests at h=4 and h=1. The viscous and shock wave regions selected are plotted in figure 3.

In figures 4, 5 and 6 the drag polars computed on the medium, fine and the superfine grid are compared with the experimental data. In the same figures it is also proposed the breakdown in viscous and wave drag. The analysis of figure 4 shows that, even for a grid with only 128 cells around the airfoil, the identification of the spurious drag contribution ($\approx$ 16 counts in this case) allows for a satisfactory prediction of $C_{D_v} + C_{D_w}$ (the total drag) on a wide range of lift coefficients (the test at C_L=0.6 is not reported because not fully converged on the medium level). For the fine level (see figure 5) the detected spurious drag is $\approx$ 5 counts, and it reduces to $\approx$ 2 counts

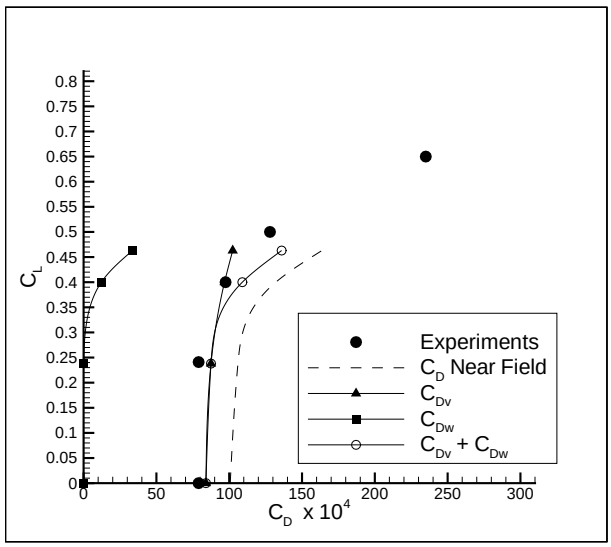

Fig. 4 NACA 0012, viscous test, comparison of the drag polars, medium grid test, $M_\infty = 0.7$, $Re_\infty = 9 \cdot 10^6$.

for the superfine level, see figure 6. In both cases the agreement of $C_{D_v} + C_{D_w}$ with the experiments is excellent. The figures also show a satisfactory agreement among the viscous and wave drag contributions as computed on the different grids. The wave drag only appears at higher lift conditions, when the up-

per shock forms and, as expected, is strongly dependent on lift. On the contrary the viscous drag dependence on lift is weaker, and significant variations of C_{D_v} only appear when the shock boundary layer interaction becomes strong.

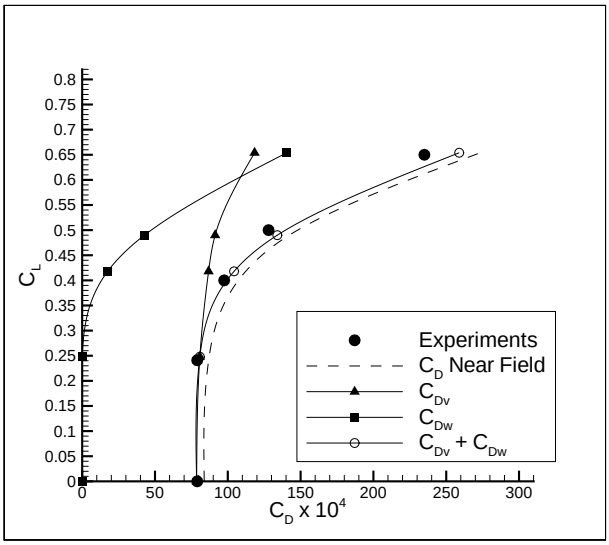

Fig. 5 NACA 0012, viscous test, comparison of the drag polars, fine grid test, $M_\infty = 0.7$, $Re_\infty = 9 \cdot 10^6$.

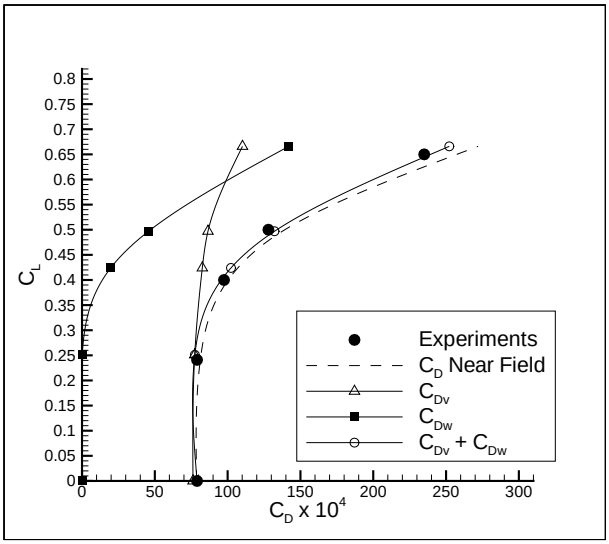

Fig. 6 NACA 0012, viscous test, comparison of the drag polars, superfine grid test, $M_\infty = 0.7$, $Re_\infty = 9 \cdot 10^6$.

4.2 Wing-Body, viscous flow

Some results obtained on a wing body transonic configuration are here presented. The free stream flow conditions are $M_\infty = 0.75$, $Re_\infty = 4.3 \cdot 10^6$. Wind tunnel experiments are presented in [16].

This test is interesting because shows the feasibility of computing and decomposing the entropy drag in the case of complex 3D flows. Furthermore it illustrates that, in practical applications (block structured grids, skewness and stretching of the grid at block interfaces), the identification of the spurious drag contribution is even more important. The used mesh is a 41 blocks grid (1600513 points on the finest level), built by NLR (the Dutch Aerospace Laboratory) in the frame of an European research project [17].

In figures 7 the computed pressure distributions are compared with the experiments for two wing sections showing an excellent agreement.

Finally in figure 8 the breakdown of the entropy drag into viscous and wave components is presented. In this case the far field drag cannot be compared with the near field value because present method does not account for the vortex drag. However, in the figure a vortex drag (C_{D_i}) estimation by a different method is also plotted. C_{D_i} has been computed by the Maskell's formula [6], [7], [11], in which the drag due to lift is related to a vorticity integral in the Trefftz plane.

The experimental polar curve cannot be considered as a reference for the validation of the present breakdown of the total drag. This is because the experiments were performed on an half model which are not well suited for the determination or the totale drag (the experiments were devoted for the computation of the engine installation drag). Furthermore a slight variation of the "numerical" C_{D_i} with the position of the Trefftz plane has been verified, indicating a small range of uncertainty for the total computed drag ($C_{D_v} + C_{D_w} + C_{D_i}$).

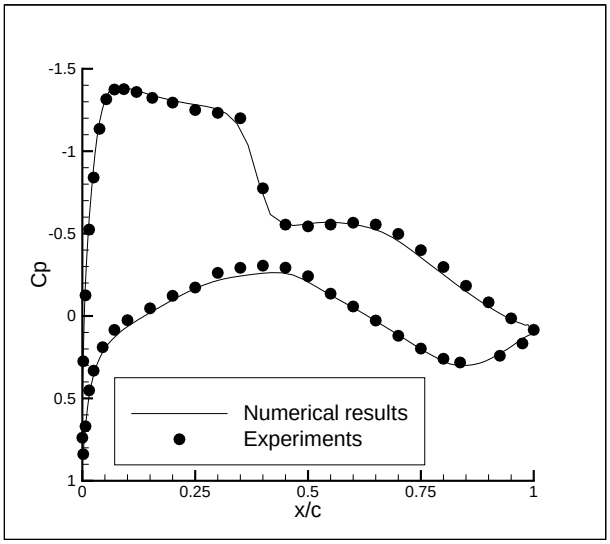

(a)

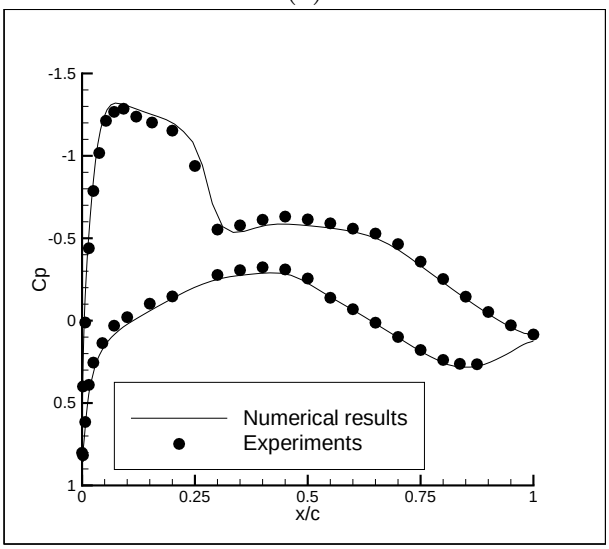

(b)

Fig. 7 Wing-Body, viscous test, surface pressure distribution at wing section $M_\infty = 0.75$, $Re_\infty = 4.3 \cdot 10^6$, C_L =0.6. (a): $\frac{y}{b/2} = 0.62$; (b): $\frac{y}{b/2} = 0.87$.

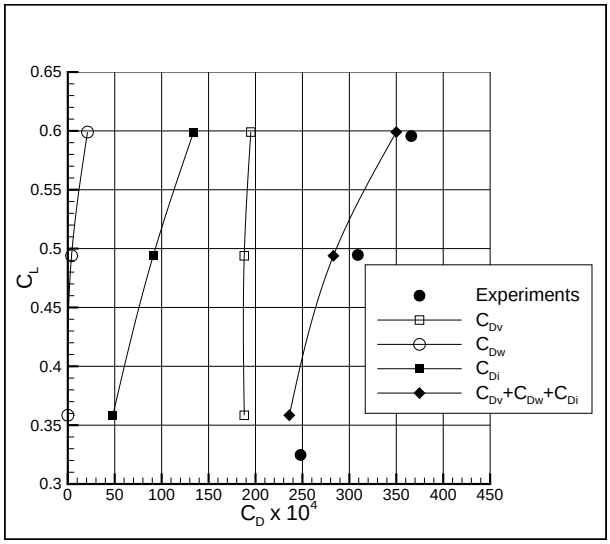

Fig. 8 Wing-Body viscous test, viscous, wave and induced drag polars, $M_\infty = 0.75$, $Re_\infty = 4.3 \cdot 10^6$.

5 Conclusions

A far field method for accurate calculations of the entropy drag is here proposed, relying on a given numerical solution of the RANS equations. The method allows for decomposition of the drag in its viscous and wave contribution once the boundary layer and the shock wave regions are identified. for this purpose a robust algorithm has been introduced for the selection of the boundary layer/wake and shock wave zones.

The method has been tested by determining the polar curves for a transonic airfoil flow with grids of different mesh size. It has been shown that the classical Oswatitsch's formula is not accurate in viscous flows, but a second order correction term, here proposed, is required. The far field drag calculation is equivalent to the near field analysis, both methods converging as mesh size becomes infinitely small. The agreement with experimental results is excellent as far as the numerical solution is accurate. Moreover, once the the boundary layer and the shock wave regions are selected, it is possible, to compute and remove a substantial part of the spurious drag introduced by the numerical dissipation of the flow solver. As consequence, the corrected drag resulted only weakly dependent on grid size implying an accurate drag calculations even on medium sized grids.

At the end the algorithm has been tested by studying a wing-body configuration in transonic flow showing the capability to analyze more complex and realistic aircraft configurations, although in this case the computation

of the total drag also requires the calculation of the vortex drag by a different method.

Aknowledgements

Present work has been partially developed in the frame of the AIRDATA (AIRcraft Drag And Thrust Analysis) Research Project funded by the EC (Contract BPR-C197-470).

References

[1] Slooff, J. W., Computational Drag Analysis and Minimization; Mission Impossible?, *Proceedings of the Aircraft Drag Prediction and Minimization Symposium*, AGARD R-723, Addendum 1, 1986.

[2] van der Vooren, J., Sloof, J. W., CFD-Based Drag Prediction; State of the Art, Theory, Prospects, *Lectures notes prepared for the AIAA Professional Studies Series, Course on Drag-Prediction and Measurement*, Portland (OR), 1990.

[3] van Dam, C. P., Recent Experience with Different Methods of Drag Prediction, *Progress in Aerospace Sciences*, Vol. 35, 1999, pp. 751-798.

[4] Oswatitsch, K., *Gas Dynamics*, Academic Press Inc, New York, 1956, pp. 177-210.

[5] Lock, R. C., The Prediction of the Drag of Aerofoils and Wings at High Subsonic Speeds, *Aeronautical Journal*, Vol. 90, No. 896, 1986, pp. 207-226.

[6] Giles, M. B., Cummings, R. M., Wake Integration for Three-Dimensional Flowfield Computations: Theoretical Development, *Journal of Aircraft*, Vol. 36, No. 2, 1999, pp. 357-365.

[7] Hunt, D. L., Cummings, R. M., Giles, M. B., Wake Integration for Three-Dimensional Flowfield Computations: Applications, *Journal of Aircraft*, Vol. 36, No. 2, 1999, pp. 366-373.

[8] Chao, D. D., van Dam, C. P., Airfoil Drag and Decomposition, *Journal of Aircraft*, Vol. 36, No. 4., 1999, pp. 675-681.

[9] Schmitt, V. Destarac, D., Recent Progress in Drag Prediction and Reduction for Civil Transport Aircraft at ONERA, AIAA paper 98-0127, Jan. 1998.

[10] Iannelli, P. L., Tognaccini, R. Drag Prediction from CFD Calculations: Formulae and Description of the Algorithms, Technical Report of the Dipartimento di Progettazione Aeronautica, Università degli Studi di Napoli "Federico II", NT 99-043, 1999.

[11] van Dam, C. P., Nikfetrat, K., Wong, K., Vijgen, P.M.H.W., Drag Prediction at Subsonic and Transonic Speeds Using Euler Methods, *Journal of Aircraft*, Vol. 32, No. 4., 1995, pp. 839-845.

[12] Martinelli, L., *Calculations of Viscous Flows with a Multigrid Method*, Ph.D. Dissertation, Mechanical and Aerospace Engineering Dept., Princeton Univ., Princeton, NJ, 1987.

[13] Baldwin, B. S., Lomax, H., Thin Layer Approximation and Algebraic Model for Separated Turbulent Flows, AIAA paper 78-257, Jan. 1978.

[14] Spalart, P. S., Allmaras, S. R., A One Equation Turbulence Model for Aerodynamics Flows, AIAA paper 92-0439, Jan. 1992.

[15] Harris, C. D., Two Dimensional Aerodynamic Characteristics of the NACA 0012 Airfoil in the Langley 8-Foot Transonic Pressure Tunnel, NASA TM 81927, 1981.

[16] ONERA Tests on the ALVAST Half Model Equipped with TPS6402, VHBR2 and CRUF2 Powered Nacelles in Test Section no 1-40 m^2 of SIMA, Wind Tunnel Test Report, TR 2/8055 DSMA/Y, February 1999.

[17] Laban, M., Aircraft Drag and Thrust Analysis (AIRDATA) Project Overview and Key Results, *Proceedings of the Workshop on EU-Research on Aerodynamic Engine/Aircraft Integration for Transport Aircraft*, DLR, Braunschweig, 2000, pp. 9-1,9-15.